

The BeppoSAX view of the X-ray active nucleus of NGC4258

F. Fiore^{1,2,3}, S. Pellegrini⁴, G. Matt⁵, L.A. Antonelli¹, A. Comastri⁶, R. Della Ceca⁷,
E. Giallongo¹, S. Mathur⁸, S. Molendi⁹, A. Siemiginowska³, G. Trinchieri⁷,
and B. Wilkes³

¹ Osservatorio Astronomico di Roma, Via Frascati 33, I-00044 Monteporzio, Italy

² BeppoSAX Science Data Center, Via Corcolle 19, I-00131 Roma, Italy

³ Harvard-Smithsonian Center of Astrophysics, 60 Garden Street, Cambridge MA 02138
USA

⁴ Dip. di Astronomia, Università di Bologna, via Ranzani 1, I-40127, Bologna, Italy

⁵ Dip. di Fisica, Università Roma Tre, via della Vasca Navale 84, I-00146, Roma, Italy

⁶ Osservatorio Astronomico di Bologna, via Ranzani 1, I-40127, Bologna, Italy

⁷ Osservatorio Astronomico di Brera, Via Brera 28, 20121, Milano, Italy

⁸ Astronomy Dept. The Ohio State University, 140 West 18th Avenue Columbus, OH
43210, USA

⁹ IFC/CNR, via Bassini 15, Milano, Italy

(version: 12 February 2001)

ABSTRACT

BeppoSAX observed the Seyfert 1.9 galaxy NGC4258 on December 1998, when its 2-10 keV luminosity was about 10^{41} erg s⁻¹. Large amplitude (100%) variability is observed in the 3-10 keV band on timescales of a few tens of thousands seconds while variability of $\sim 20\%$ is observed on timescales as short as one hour. The nuclear component is visible above 2 keV only, being obscured by a column density of $(9.5 \pm 1.2) \times 10^{22}$ cm⁻²; this component is detected up to 70 keV with a signal to noise $\gtrsim 3$, and with the steep power law energy spectral index of $\alpha_E = 1.11 \pm 0.14$. Bremsstrahlung emission for the 2-70 keV X-ray luminosity, as expected in Advection Dominated Accretion Flow (ADAF) models with strong winds, is ruled out by the data. The ratio between the nuclear radio (22 GHz) luminosity and the X-ray (5 keV) luminosity is $\lesssim 10^{-5}$, similar to that of radio-quiet quasars and Seyfert galaxies. X-ray variability and spectral shape, radio-to-X-ray and near infrared-to-X-ray luminosity ratios suggest that the nucleus of NGC4258 could be a scaled-down version of a Seyfert nucleus, and that the X-ray nuclear luminosity can be explained in terms of Comptonization in a hot corona.

The soft ($E \lesssim 2$ keV) X-ray emission is complex. There are at least two thermal-like components with temperatures of 0.6 ± 0.1 keV and $\gtrsim 1.3$ keV. The

cooler ($L_{0.1-2.4keV} \sim 10^{40}$ erg s $^{-1}$) component is probably associated with the jet, resolved in X-rays by the ROSAT HRI (Cecil et al. 1994). The luminosity of the second component, which can be modeled equally well by an unobscured power law model with $\alpha_E = 0.2_{-0.2}^{+0.8}$, is $L_{0.1-2.4keV} \sim 7 \times 10^{39}$ erg s $^{-1}$, consistent with that expected from discrete X-ray sources (binaries and SN remnants) in the host galaxy.

Observations of NGC4258 and other maser AGNs show strong nuclear X-ray absorption. We propose that this large column of gas might be responsible for shielding the regions of water maser emission from X-ray illumination. So a large column density absorbing gas may be a necessary property of masing AGNs.

Subject headings: Galaxies: Seyfert – Galaxies: individual: NGC4258 —
X-rays: galaxies

1. Introduction

The nearby (distance of 7.2 ± 0.3 Mpc, Herrnstein et al. 1999), bright ($B_0^T = 8.5$), SABbc galaxy NGC4258 (M106) is spectroscopically classified as a 1.9 Seyfert galaxy (Ho, Filippenko & Sargent 1997, who find $[OIII]/H\beta=10.3$, and $[SII]/H\alpha=0.94$). Wilkes et al. (1995) find relatively broad (1000 km s $^{-1}$) emission lines, which are strongly polarized (5-10%), supporting the existence of an obscured active nucleus in this galaxy. Further support to this case comes from high resolution observations of the water maser in the galaxy nucleus. Miyoshi et al. (1995) discovered a highly inclined thin disk between 0.13 and 0.25 pc. The inclination of the disk is estimated to 82 ± 1 degrees (Herrnstein et al. 1999, the inclination of the galaxy is 70 degrees, Ho et al. 1997). The aspect ratio of the disk is extremely small, $\lesssim 0.2\%$ (Herrnstein et al. 1999). The Keplerian rotation curve traced by the water maser requires a central binding mass, presumably in the form of a supermassive black hole, of $3.9(\pm 0.1) \times 10^7 M_\odot$ (Herrnstein et al. 1999). To date, this is the strongest evidence for a supermassive black hole in a galaxy and the best measurement of its mass. The implied Eddington luminosity is $\sim 5 \times 10^{45}$ erg s $^{-1}$. Pending an accurate estimate of the observed nuclear luminosity, it is therefore possible in this case to constrain tightly the L/L_{Edd} ratio of the active nucleus.

The evaluation of the nuclear luminosity and spectrum is not an easy task because the nucleus is highly obscured. Wilkes et al. (1995) discovered a faint, blue, highly polarized nuclear continuum, but the uncertainty on the optical nuclear luminosity is large

(two orders of magnitude, depending on the nature of the scattering region). Similar uncertainties are found using the intensity of the emission lines. Chary & Becklin (1997) found a “nuclear” emission at 2 micron, in excess of that expected from the galaxy profile, of 4.5 mJy, corresponding to a luminosity ($\nu L(\nu)$) of about 10^{41} erg s $^{-1}$. The nucleus is not detected in VLBA radio maps. Herrnstein et al. (1998) report upper limits to the 22 GHz flux and luminosity of 0.22 mJy and $\nu L(\nu) = 3 \times 10^{35}$ erg s $^{-1}$ respectively. Conversely, a double, twisted radio jet is visible on scales from milliarcsec to a few arcmin (the latter scale corresponding to a few kiloparsec at the galaxy distance). The jets are visible in optical and X-ray images too. In particular, Cecil, Wilson & De Pree (1995) resolved the jets in ROSAT HRI observations and measured a 0.1-2.4 keV luminosity of 6.5×10^{39} erg s $^{-1}$. They also detected an unresolved “nuclear” emission of comparable luminosity, confirming previous Einstein results (Fabbiano et al. 1992). ASCA spectra (Makishima et al. 1994, Ptak et al. 1999, Reynolds et al. 2000) resolve at least two distinct components, a thermal component dominating the spectrum up to 2-3 keV and a highly absorbed power law dominating the spectrum above this energy. The ASCA power law energy index is $\alpha_E \sim 0.8$ and the neutral absorbing column is in the range $N_H = (0.9 - 1.5) \times 10^{23}$ cm $^{-2}$ (see Reynolds et al. 2000 for details). The 2-10 keV flux observed by ASCA varied between 3×10^{-12} and 10^{-11} erg cm $^{-2}$ s $^{-1}$ (Reynolds et al. 2000), $(6-15) \times 10^{-12}$ erg cm $^{-2}$ s $^{-1}$, when corrected for intrinsic absorption, during several observations performed between May 1993 and May 1999. This implies a 2-10 nuclear luminosity in the range $(0.4 - 1) \times 10^{41}$ erg s $^{-1}$. The uncertainties on the spectral index and absorbing column are quite large (0.2–0.3 and $(1 - 2) \times 10^{22}$ cm $^{-2}$ respectively), due to the fact that only a narrow energy band is unaffected by the bright thermal component, and so is the uncertainty on the unobscured flux. Reynolds et al. (2000) also report the detection of a narrow 6.4 keV iron K α line of equivalent width of 107_{-37}^{+42} eV.

Because of the small luminosity in terms of the Eddington one, the nuclear emission of NGC4258 can be explained either by a standard accretion disk with a very small accretion rate, or by radiatively inefficient accretion models, such as the Advection Dominated Accretion Flows (ADAF, e.g. Narayan & Yi 1995). The Radio to X-ray Spectral Energy Distribution (SED) has been interpreted in terms of emission from an ADAF with a critical accretion rate $\dot{m} \sim 0.016\alpha_{-1}$ (Lasota et al, 1996; α_{-1} is the viscosity parameter in units of 0.1) or $\dot{m} \sim 0.012\alpha_{-1}$ (Gammie et al. 1999, their modeling also includes the NIR data and the 22 GHz upper limit). In ADAF models the radio luminosity comes from synchrotron emission and the X-ray comes from the combined contributions of a high temperature (kT \gtrsim 100 keV) thermal bremsstrahlung and Comptonization of the synchrotron photons. Lasota et al. (1996) point out that this representation is not unique, because of the substantial uncertainties in the optical-UV and X-ray data and because of the difficulty

in distinguishing an ADAF from thermal Comptonization, using only the X-ray spectral shape. Both Lasota et al. (1996) and Gammie et al. (1999) do not account in their models for the strong wind expected from the inner accretion disk (Blandford & Begelman 1999, Di Matteo et al. 2000). The wind carries a significant fraction of the mass, energy and angular momentum. In particular, it drastically reduces the synchrotron emission in the radio band and the Compton emission in the O-UV and X-ray bands (Di Matteo et al. 2000). In both modelings the NIR luminosity is generated by a standard, geometrically thin disk, external to the ADAF transition radius.

BeppoSAX, with its good sensitivity over a broad (0.1-200 keV) band, can help in separating the different X-ray spectral components and can provide a strong constraint on the nuclear power law spectral index and on the high energy cut-off (predicted by both ADAF models and thermal Comptonization models). It can help understanding whether the NGC4258 nucleus hosts a “normal” AGN (although of low luminosity) or rather an ADAF. BeppoSAX observed NGC4258 for about 100 ks on December 19-22 1998. The nuclear component was in a high state in comparison with most ASCA observations. This, together with the broad band (the source is detected with a signal to noise ratio $\gtrsim 3$ up to about 70 keV) allows us to tightly constrain the flux and spectral shape of the nuclear hard component.

The paper is organized as follows: Section 2 presents the data and gives information on their reduction; Section 3 presents a variability analysis; Section 4 presents the spectral analysis and the broad band, radio to X-ray spectral indices; Section 5 discusses the main results on the hard nuclear component and on the low energy components.

2. Observation and data reduction

The observations were performed with the BeppoSAX Narrow Field Instruments, LECS (0.1-10 keV, Parmar et al. 1997), MECS (1.3-10 keV, Boella et al. 1997b), HPGSPC (4-60 keV, Manzo et al. 1997) and PDS (13-200 keV, Frontera et al. 1997). LECS and MECS are imaging gas scintillation proportional counters, the HPGSPC is a collimated high pressure gas scintillation proportional counter and the PDS consists of four phoswich units. The PDS is operated in the so called “rocking mode”, with a pair of units pointing to the source while the other pair monitor the background ± 210 arcmin away. The units on and off source are interchanged every 96 seconds. We report here the analysis of the LECS, MECS and PDS data; the HPGSPC data are very noisy, due to high HPGSPC background. The MECS observations were performed with units 2 and 3 (on 1997 May 6th a technical failure caused the switch off of unit MECS1); these data were combined together after gain

equalization. The LECS is operated during dark time only, therefore LECS exposure times are usually smaller than MECS ones (a factor of 3 for NGC4258). Table 1 gives the LECS, MECS and PDS exposure times and the count rates.

Standard data reduction was performed using the SAXDAS software package version 2.0 following Fiore, Guainazzi and Grandi (1999). In particular, data are linearized and cleaned from Earth occultation periods (we accumulated data for Earth elevation angles > 5 degrees) and unwanted periods of high particle background (satellite passages through the South Atlantic Anomaly and periods with magnetic cut-off rigidity > 6 GeV/c). The internal background of the LECS, MECS and PDS during the accepted periods is relatively low and stable (variations at most of 30% during the orbit) due to the low inclination of the satellite orbit (3.95 degrees). LECS and MECS spectra were extracted from regions of 8 arcmin and 3 arcmin radii respectively. These radii maximize the signal-to-noise ratio below 1 keV in the LECS and above 2 keV in the MECS. Background spectra were extracted in detector coordinates from high Galactic latitude ‘blank’ fields (98_11 issue) using regions equal in size to the source extraction region. We have checked that the mean level of the background in the LECS and MECS “blank fields” observations is comparable with the mean level of the background in the NGC4258 observations using source free regions at various positions in the detectors.

The PDS data have been reduced using the variable Risetime threshold technique to reject particle background (see Fiore, Guainazzi & Grandi 1999). This technique reduces the total 13-200 keV background to about 20 counts s^{-1} and the 13-80 keV background to about 6 counts s^{-1} (instead of 30 and 10 counts s^{-1} respectively, obtained using the standard fixed Risetime threshold technique). The PDS rocking mode provides a very reliable background subtraction. This can be checked looking at the spectrum between 200 and 300 keV, where the effective area of the PDS to X-ray photons is small and therefore the source contribution is negligible; we obtain after background subtraction 0.0085 ± 0.012 counts s^{-1} , consistent with the expected value of 0. The net (background subtracted) 13-130 keV on-source signal is 0.121 ± 0.024 counts s^{-1} . The source is detected with a signal to noise ratio $\gtrsim 3$ up to ~ 70 keV. The 13-130 keV PDS count rate is $\gtrsim 3.5$ times the systematic uncertainty in the PDS background subtraction, equal to 0.020 ± 0.015 , (Guainazzi & Matteuzzi 1997). Confusion in the PDS collimator Field Of View (1.4 degrees FWHM) ultimately limits our capability to constrain the high energy spectrum. We have carefully checked for any possible contaminant in a region of 1.5 degrees radius around NGC4258 (using the NED, SIMBAD, AGN, clusters, CVs, Radio and X-ray sources catalogs) finding no obvious bright hard X-ray source. Of course there is the possibility of a bright “unknown” source in the PDS field of view. The chance of finding a source in any given 2 square degrees, the PDS beam area, is however small. The HEAO-1 A4 all sky catalog (Levine et al. 1984) lists

just 7 high Galactic latitude sources in the 13-80 keV band down to a flux of 2×10^{-10} erg $\text{cm}^{-2} \text{s}^{-1}$ (10mCrab). The 13-80 keV flux is about 20 times smaller than this figure and so, assuming a logN-logS slope of -1.5 , we expect a chance coincidence rate of 2%.

Table 1: **Observation log for BeppoSAX sequence 50491001**

Instrument	Exposure (ks)	Band	Count rate
LECS	33.3	0.1-4 keV	3.00 ± 0.11^a
MECS	99.4	1.7-10 keV	7.25 ± 0.09^a
PDS	46.9	13-130 keV	0.121 ± 0.024

^a 10^{-2} counts s^{-1}

3. Variability

Figure 1 shows the MECS 3-10 keV light curve in bins of 2850 seconds. Variability of a factor of about two is evident on timescales of half day, as well as smaller amplitude variations (10-20 %) on time scales as short as one hour. Shorter timescales variations of similar amplitude cannot be sampled, due to the limited sensitivity of the MECS instrument. In this regard the source behaves in a way similar to X-ray brighter, and better studied, Seyfert galaxies (e.g. NGC4051, NGC5506, Green et al. 1993, Nandra et al. 1997).

Figure 2 shows the MECS 3-5 keV and 5-10 keV light curves (on the same scale), together with their ratios. The light curves are not background subtracted (the internal+cosmic background is about 3% and 6% of the mean total count rate in the two bands, and therefore it is negligible). The two MECS lightcurves present similar but not identical variations and, in fact, their hardness ratio shows small ($\lesssim 20\%$) variations. Unfortunately the statistic is not good enough to perform an accurate spectral variability study. To this purpose high throughput instruments, like those that are on board the Chandra and XMM-Newton satellites, are needed. In any case, the spectral variations are expected to be small enough to allow us to safely use time integrated counts. We therefore concentrate hereinafter on the time averaged properties of the spectrum.

4. Spectral analysis

Spectral fits were performed using the XSPEC 9.0 software package and public response matrices as from the 1998 November release. LECS and MECS spectra were rebinned following two criteria: a) to sample the energy resolution of the detectors with four channels

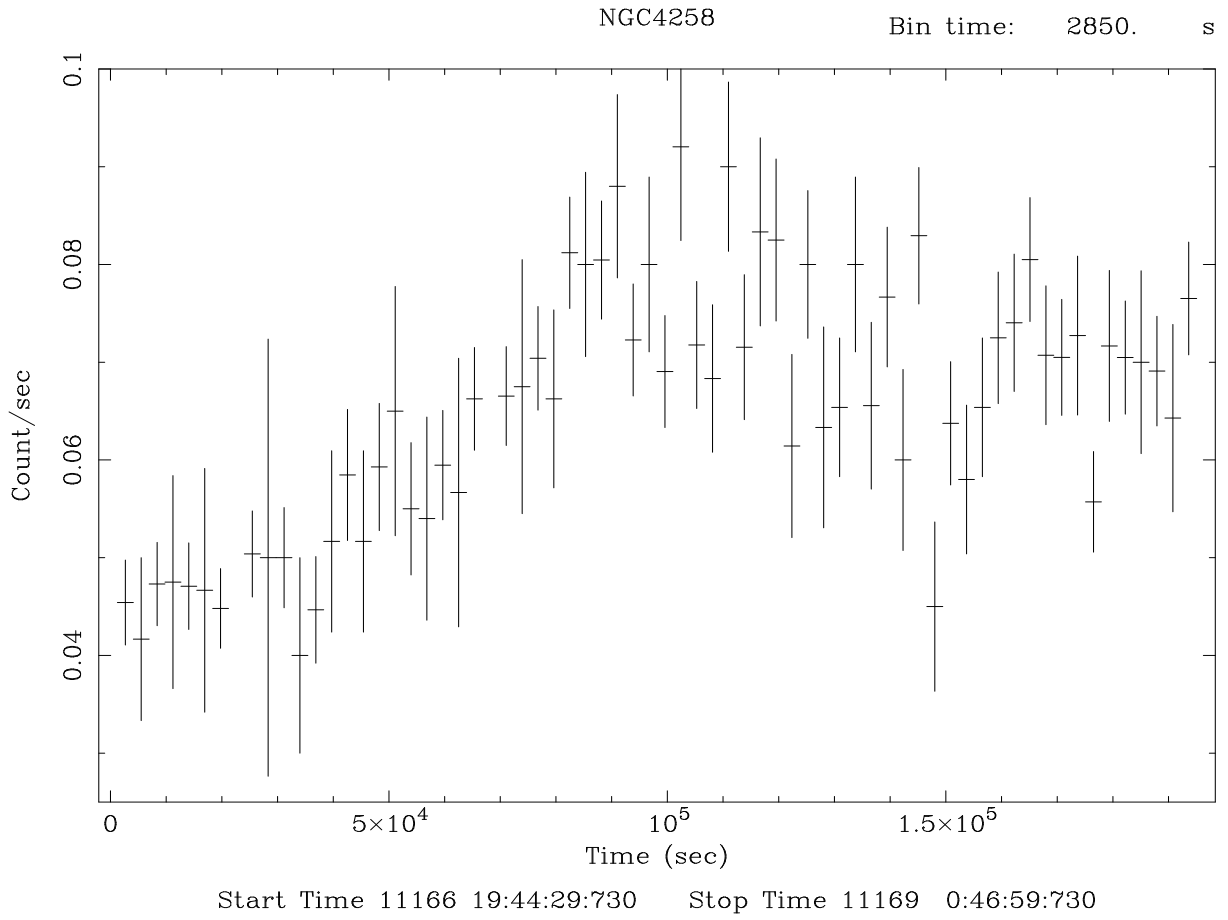
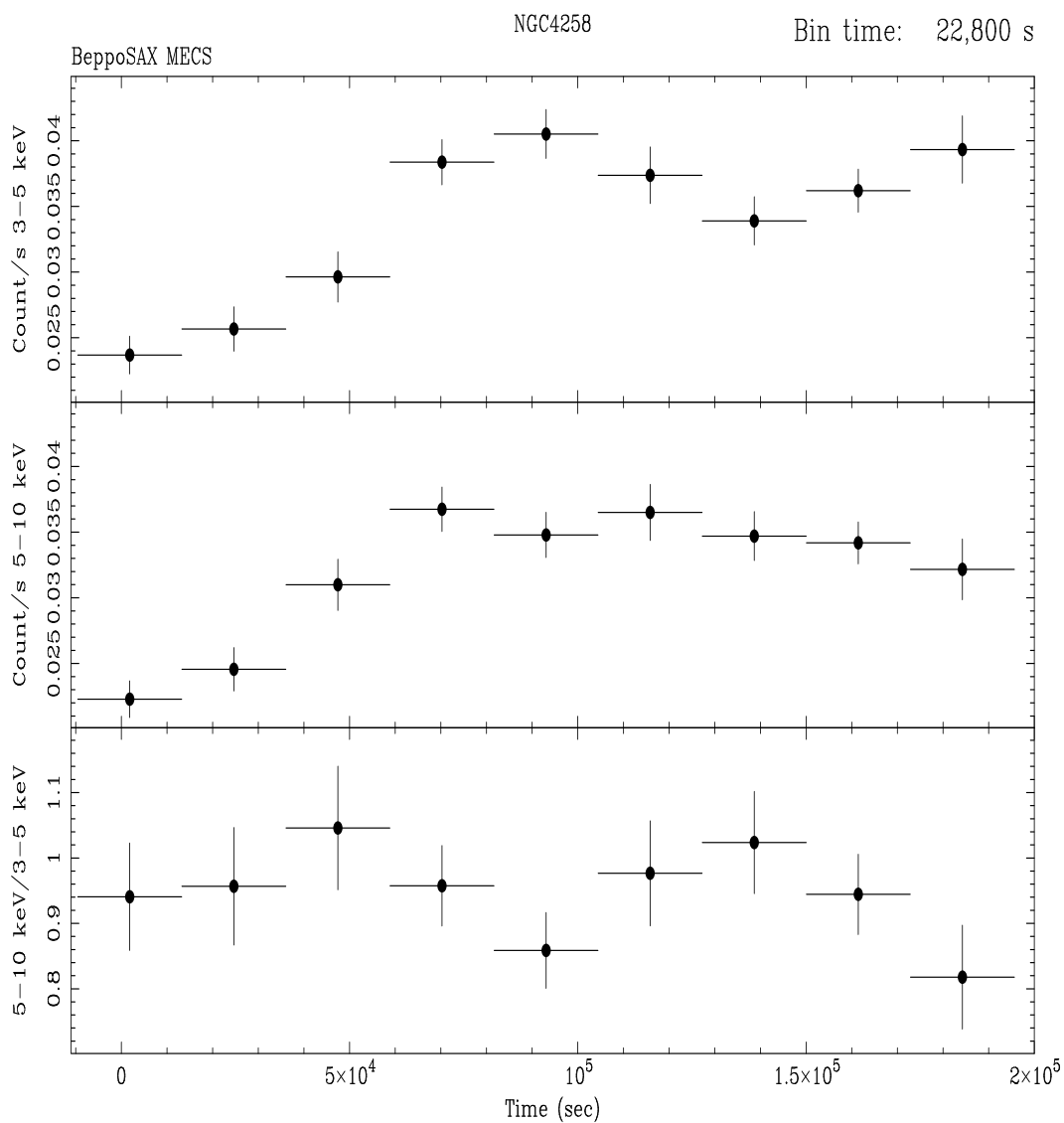


Fig. 1.— The BeppoSAX MECS 3-10 keV light curves of NGC4258 in bins of 2850 seconds (half satellite orbit). Errors represent the 1σ confidence interval.



Start Time 11166 22:30:44:730 Stop Time 11169 1:10:44:730

Fig. 2.— The BeppoSAX MECS light curves of NGC4258 in the 3-5 keV and 5-10 keV bands (upper and middle panels, bins of 22800 seconds, corresponding to about 4 satellite orbits per bin). The 5-10keV/3-5keV count ratio as a function of time (lower panel).

at all energies whenever possible, and b) to obtain at least 20 counts per energy channel. Constant factors have been introduced in the fitting models in order to take into account the intercalibration systematics between the instruments. The expected factor between LECS and MECS is about 0.9 [0.7-1.1]; the factor between the PDS and MECS is 0.8 [0.7-0.9] (see Fiore, Guainazzi & Grandi 1999). We assume in all spectral fits the MECS as reference instrument. The energy range used for the fits are: 0.1-4 keV for the LECS (channels 11-400), 1.65-10 keV for the MECS (channels 37-213) and 13-100 keV for the PDS. Errors quoted in this paper are 90% confidence intervals for one interesting parameter ($\Delta\chi^2 = 2.71$).

Figure 3 shows that the 0.1-100 keV spectrum (LECS+MECS+PDS) is highly complex. A strong cut-off below 4 keV is clearly visible as well as a faint emission line feature between 6 and 7 keV. The large excess visible between 0.7 and 1 keV is likely due to iron L emission from an optically thin plasma. The next Section presents the analysis of the high energy spectrum ($E > 2.5$ keV). The thermal component(s) dominating the spectrum below ~ 2 keV are discussed in Section 4.2.

4.1. The hard nuclear component

The intensity of the hard component is strongly reduced by photoelectric absorption below 2-3 keV. For the sake of simplicity we therefore exclude the LECS data and limit the fit to the MECS+PDS data above 2.5 keV, when considering the nuclear component. The MECS+PDS spectra were fitted with a power law model plus photoelectric absorption. The agreement between the data and this simple model is acceptable (see Table 2). Thanks to the broad energy band the power law spectral index and the column density of the absorbing gas are well constrained ($\alpha_E = 1.11 \pm 0.14$, $N_H = 0.95(\pm 0.12) \times 10^{23} \text{ cm}^{-2}$). Figure 4 shows the ratio between the MECS and PDS data and the best fit model.

The observed 2-10 keV flux is $8.0 \times 10^{-12} \text{ erg cm}^{-2} \text{ s}^{-1}$, while the flux corrected for intrinsic absorption is $1.52(\pm 0.15) \times 10^{-11} \text{ erg cm}^{-2} \text{ s}^{-1}$. The uncertainty on the unabsorbed flux is mostly due to the uncertainty on the absorbing column. The 2-10 keV nuclear (unobscured) luminosity is $1.0(\pm 0.1) \times 10^{41} \text{ erg s}^{-1}$. The broad band 0.1-100 keV luminosity of the hard component is $4.5 \times 10^{41} \text{ erg s}^{-1}$.

The inclusion of a narrow line is significant at the 98% confidence level according to the F test. The line energy (6.57 ± 0.20 keV) is consistent with $K\alpha$ emission from both neutral and helium like iron. The equivalent width (85 ± 65 eV) is not well constrained. It is consistent with but somewhat lower than that of Seyfert 1 and Compton thin Seyfert 1.9-2

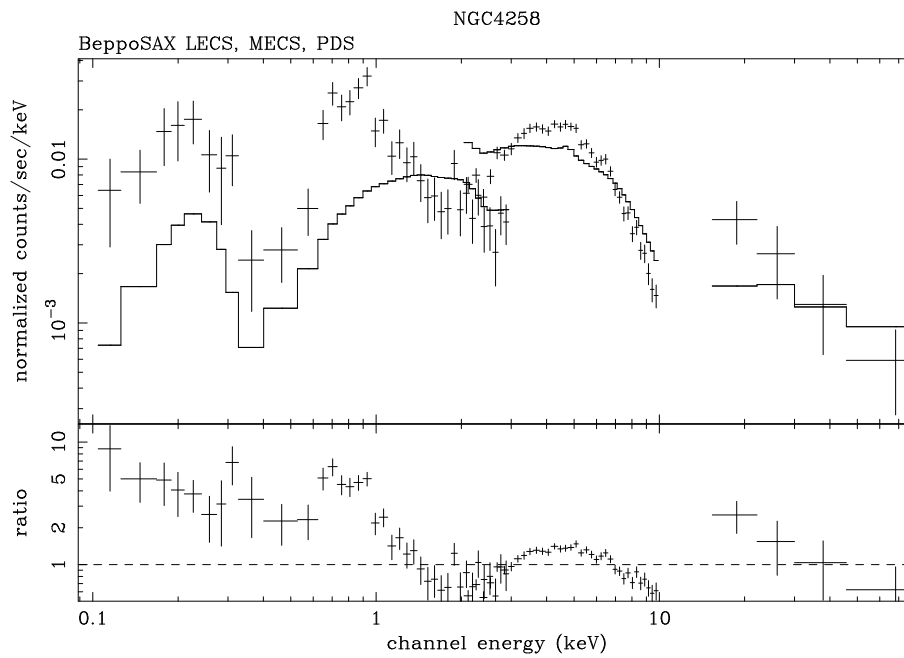


Fig. 3.— The 0.1-100 keV BeppoSAX LECS, MECS and PDS spectra of NGC4258 fitted with a single power law model in the full 0.1-100 keV band. Note the strong cut-off below 4 keV and the large excess between 0.7 and 1 keV (likely due to iron L emission from an optically thin plasma).

galaxies (Matt 2000). Assuming neutral iron, the observed equivalent width is consistent with that expected from transmission through a column density of about 10^{23} cm^{-2} (Ghisellini, Haardt & Matt 1994). The inclusion of a high energy cut-off is not significant. The 90% confidence level lower limit to the cut-off energy is 30 keV.

We have also fitted the MECS and PDS data with a thermal bremsstrahlung model (table 2). The χ^2 is significantly worse than in the power law model fit. We have then fitted the data with a power law plus bremsstrahlung model (fixing the temperature of the bremsstrahlung to 100 keV), to put a limit on the flux of an additional spectral component with the shape predicted by ADAF models with strong winds. The 90% limits on the 2-10 keV unabsorbed flux and on the 0.1-100 keV luminosity of this component are $4 \times 10^{-12} \text{ erg cm}^{-2} \text{ s}^{-1}$ and $1.5 \times 10^{41} \text{ erg s}^{-1}$ respectively, about one third of the total 0.1-100 keV nuclear luminosity.

Table 2: **Spectral fits: 2.5-100 keV band**

model	N_H^a	α_E or kT^b	line E ^b	line EW ^c	$\chi^2(\text{dof})$
Power Law	9.5 ± 1.2	1.08 ± 0.14			30.3(40)
Power Law + line	9.4 ± 1.2	1.11 ± 0.14	6.57 ± 0.20	85 ± 65	25.3(38)
Brem.	$7.9^{+0.7}_{-1.3}$	$9.5^{+3.5}_{-1.2}$			40.7(44)

^a in 10^{22} cm^{-2} ; ^b in keV; ^c in eV

Table 3: **Spectral fits: 0.1-100 keV band**

model	kT_1^a	kT_2^a or α_{E2}	A_1^b	A_2^b	Flux ₁ ^c	Flux ₂ ^c	$\chi^2(\text{dof})$
MEKAL+PL+line	0.81 ± 0.07	–	0.11 ± 0.05		2.0	–	108.9 (92)
2 MEKAL+PL+line	$0.6^{+0.07}_{-0.20}$	> 1.3	> 0.2	< 0.9	1.7, 0.03	1.1, 0.6	87.3(89)
MEKAL+2PL+line	0.6 ± 0.1	$0.2^{+0.8}_{-0.2}$	> 0.2	–	1.6, 0.04	0.4, 2.0	85.3 (90)
MEKAL+2PL+line ^d	0.6 ± 0.1	1.05 ± 0.08	> 0.2	–	1.0, 0.02	1.3, 0.90	89.6 (91)

^a in keV; ^b metal abundance in unit of solar abundance; ^c 0.1-2.4 and 2-10 keV fluxes in $10^{-12} \text{ erg cm}^{-2} \text{ s}^{-1}$; ^d the spectral indices of the obscured and unobscured power laws are linked together

4.2. The low energy spectrum

To study the low energy spectrum of NGC4258 we now include in the spectral fitting the MECS data in the full 1.7-10 keV band and the LECS spectrum, which covers the 0.1-4 keV band. The LECS, MECS and PDS data were fitted with an optically thin thermal plasma model (MEKAL) plus the nuclear absorbed power law component and an iron K α line. An additional absorbing column of density fixed to the Galactic value along the line of

sight ($N_H = 1.16 \times 10^{20} \text{ cm}^{-2}$) has been included in the fit. The best fit power law spectral index and intrinsic absorption resulted very close to the best fit values found in the previous section. In Table 3 we give only the parameters of the low energy component.

The fit with a single thermal component is not completely satisfactory (see Figure 5, upper panel), with rather large residuals between 0.5 and 1 keV. The LECS and MECS spectra have therefore been fitted with a two temperature model plus the highly absorbed power law and the iron $K\alpha$ line (figure 5, lower panel). The improvement in χ^2 is significant ($\Delta\chi^2 = 21.6$ for three additional parameters, corresponding to a probability of 99.98%, according to the F test, see Table 3). While the temperature of the cooler component is well constrained, for the hotter component we obtain only a lower limit of about 1.3 keV. The metal abundance of the cooler component is constrained to be higher than 0.2 solar, while that of the hot component is constrained to be smaller than 0.9 solar. The results on the other parameters do not change fixing the metal abundances to the solar value. The 0.1-2.4 keV luminosities of the cool and hot components are about 10 and $7 \times 10^{39} \text{ erg s}^{-1}$, respectively. The 2-10 keV luminosity of the hot component is $\sim 4 \times 10^{39} \text{ erg s}^{-1}$. Because of the complexity of the model and of the limited energy resolution of the LECS and the MECS the uncertainties on these values are however rather large, the order of 50%. A slightly better fit is obtained by replacing the thermal “hot” component with an unobscured power law. In this case the improvement in χ^2 is significant at the 99.998% confidence level ($\Delta\chi^2 = 23.6$ for two additional parameters). Fixing the spectral index of the unobscured power law to that of the obscured nuclear component (so mimicking a partial covering model) produces a χ^2 of 89.6, still acceptable. The covering fraction is in this case 0.935 ± 0.010 .

4.3. Comparison with previous ROSAT and ASCA observations

The BeppoSAX 2-10 keV flux is about 2 times higher than in the May 1993 and May 1999 ASCA observations, while it is similar to that in the 1996 observations (Reynolds et al. 2000). The power law index is consistent with the ASCA measurements. The column density measured by Makishima et al. (1994) is $1.5(\pm 0.2) \times 10^{23} \text{ cm}^{-2}$, while Ptak et al. (1999) find a nominally lower value $(0.5 - 0.7) \times 10^{23} \text{ cm}^{-2}$ with a typical statistical error of $(+0.8 - 0.3) \times 10^{23} \text{ cm}^{-2}$, see their tables 5 and 7. Reynolds et al. (2000) report values between 0.88 and $1.4 \times 10^{23} \text{ cm}^{-2}$. The BeppoSAX measurement is consistent with all ASCA measurements except that in the May 1993 observation.

The temperatures and abundances of the low energy components are consistent with ASCA (Makishima et al. 1994, Ptak et al. 1999, Reynolds et al. 2000) and ROSAT (Pietsch

et al. 1994, Cecil, Wilson and De Pree 1995) determinations; the luminosity of the “cool” component is in agreement with the PSPC, HRI and ASCA measurements. The luminosity of the “cool” and “hot” components are slightly higher than in the ROSAT PSPC and HRI observations and in the ASCA observations, if taken at the face value, but the uncertainties in both the BeppoSAX data on these luminosities are rather large (30 to 50%). The energy and equivalent width of the iron line are consistent with the ASCA determination.

4.4. The radio to X-ray nuclear Spectral Energy Distribution

As said in the introduction the SED of NGC4258 was compared with broad band ADAF models by Lasota et al. (1996) and Gammie et al. (1999). The fit of detailed ADAF models to the radio to X-ray SED is beyond the scope of this paper. Here we limit ourselves to consider the two broad band spectral ratios $R_{RX} = L(22\text{GHz})/L(5\text{keV})$ and $R_{NIRX} = L(2\mu)/L(5\text{keV})$, plotted in figure 6. The NGC4258 BeppoSAX and ASCA data have been combined with the Herrnstein et al. (1998) 22 GHz upper limit and with the Chary & Becklin (1997) 2μ “nuclear” emission. The resulting ratios are compared with the analogous ratios built from the Di Matteo et al. (2000) best fit ADAF + wind models to the SEDs of six nearby elliptical galaxies; and with the ratios computed from the average SEDs of UVX selected radio quiet quasars (Elvis et al. 1994). From figure 6 we note that the NGC4258 points are in the region occupied by radio quiet AGN; and that the R_{RX} and R_{NIRX} values are 2-4 orders of magnitude lower and higher, respectively, than in ADAF plus wind best fit models.

5. Discussion and Conclusions

5.1. Origin of the nuclear emission

The nuclear luminosity $L(2-10\text{ keV})$ of NGC4258 during the BeppoSAX observation was about $10^{41}\text{ erg s}^{-1}$, similar to the NIR 2μ luminosity estimated by Chary & Becklin (1997). This is consistent with an extrapolation of the X-ray power law down to a few microns. On the high energy side, the BeppoSAX data are not able to provide a strong constraint on the cut-off. However, BeppoSAX measured a cut-off energy of 100-200 keV in half a dozen Seyfert galaxies (Matt 2000 and references therein; see also Zdziarski et al. 2000, and references therein, for GRO/OSSE results). It is therefore reasonable to assume that the nuclear power law component can be extrapolated up to $\sim 200\text{ keV}$. If this is the case the 3 micron to 200 keV total nuclear luminosity is of the order of $10^{42}\text{ erg s}^{-1}$. The

uncertainty on this number strongly depends on the assumed NIR to X-ray spectral index (an uncertainty of 0.2 on this spectral index would imply a 50% uncertainty on the total luminosity). The nuclear NIR to X-ray luminosity is similar to the minimum *bolometric* luminosity implied by the Wilkes et al. (1995) detection of polarized flux. A nuclear NIR to X-ray luminosity of 10^{42} erg s $^{-1}$ and a black hole mass of $3.9(\pm 0.1) \times 10^7 M_{\odot}$ (Herrnstein et al. 1999) imply an Eddington ratio of ≈ 0.0002 . Although higher than the Eddington ratios estimated by Lasota et al. (1996) and Gammie et al. (1999) this is still in the ADAF regime (e.g. Narayan, Mahadevan & Quataert 1998). We therefore discuss briefly in the following the applicability of ADAF models to the nuclear emission of NGC4258.

The SED of ADAF models depends on a variety of parameters and assumptions (Narayan, Mahadevan & Quataert 1998, Quataert & Narayan 1999, Di Matteo et al. 2000). Here we distinguish between two main families of models, (a) those in which strong winds efficiently deplete the emission region of emitting electrons and reduce the synchrotron radio emission together with the inverse Compton emission in X-rays (e.g. Di Matteo et al 2000), and (b) those without winds. The observed 2.5-70 keV spectral index ($\alpha_E = 1.11 \pm 0.14$) is steeper than what expected in ADAF models where the contribution of Comptonization is negligible and the X-ray luminosity is mostly due to thermal bremsstrahlung with $kT=100-200$ keV, i.e. $\alpha_E \approx 0.3$ at energies below 50-100 keV (case (a), see e.g. di Matteo et al. 2000). An additional $kT \approx 100$ keV bremsstrahlung component can contribute for at most one third of the broad band X-ray luminosity of the main ($\alpha_E = 1.11$) power law component (see Sect. 4.1).

On the other hand, if the X-ray band is dominated by Comptonization, case (b), the observed X-ray spectral index can be easily explained. In this case we would expect either strong synchrotron emission in the radio band, or strong infrared emission from the outer thin disk, to provide enough soft photons for the inverse Compton scattering. We discuss these two possibilities in turn.

Strong synchrotron emission

Given the X-ray luminosity observed by ASCA and the higher one observed by BeppoSAX, the Herrnstein et al. (1998) 22GHz upper limit is barely consistent with the Gammie et al. (1999) ADAF models without wind. Furthermore, the observed radio-to-X-ray luminosity ratio is 2–3 orders of magnitude lower than in nearby elliptical galaxies supposed to host an ADAF (see Figure 6 and Sect. 4.4). ADAF solutions with or without winds seem more “radio-loud” than the NGC4258 nucleus. Conversely, the radio-to-X-ray luminosity ratio is consistent with that found in radio-quiet AGNs (Elvis et al. 1994). We also note that the 22GHz upper limit is consistent with the luminosity of a radio jet, whose power is proportional to the optical luminosity of a standard accretion disc

(as inferred from the optical emission lines, Falcke & Biermann 1999).

Strong Infrared emission

The NIR to X-ray ratio of NGC4258 is also similar to that of radio-quiet AGNs (see figure 6), while it is higher than in the Di Matteo et al. (2000) ADAF models with winds by 2-4 orders of magnitude. In fact, Gammie et al. (1999) associate the strong nuclear NIR luminosity detected by Chary & Becklin (1997) to emission from a thin disc extending down to 5-50 Schwarzschild radii ($R_S = 2GM/c^2$). According to Gammie et al. (1999) the flow should become advection dominated and produce a geometrically thick configuration at this transition radius. The size of the X-ray emission region and therefore the putative transition radius can be constrained through X-ray variability studies. There are at least two relevant timescales here, the local dynamical timescale $t_d = R^{3/2}(GM)^{-1/2}$ and the causality timescale $t_c = R/c$. Large variations on timescales of $\sim 40,000$ seconds are present in the 3-10 keV light curve of NGC4258, as well as 10-20% variations on shorter (~ 1 hour) timescales. Associating the longer timescales to t_d , as expected if the hard X-ray luminosity is mostly due to bremsstrahlung emission, produces an emission radius in units of R_S of $r \lesssim 17$. Associating the same timescale to t_c produces $r \lesssim 100$. These radii are still consistent with the ADAF transition radius of $\sim 5 - 50R_S$ suggested by Gammie et al. (1999). We note however, that even if a transition radius as small as $5R_S$ may be mathematically correct, it is less than two times the last stable orbit in a Schwarzschild metric. Since the transition between a geometrically thin disk to a thick configuration is unlikely to be very sharp, this leaves little space for the putative hot plasma region responsible for the X-ray emission. Reynolds et al. (2000) suggest that the size of the nuclear X-ray source may be as large as $\sim 50R_S$, based on the limit on the width of the iron $K\alpha$ line. However, a sizeable fraction of the line emission may well be produced by outer gas, as for example the gas responsible for the X-ray absorption, see Sect. 4.1.

In conclusion, ADAF models with strong winds can be ruled out for the nuclear emission of NGC4258, based on both the measured X-ray spectral shape and the X-ray variability. ADAF models without strong winds may be applicable but it is not clear if they are a viable physical solution (Blandford & Begelman 1999, Di Matteo et al. 2000). Moreover, they imply a radio to X-ray ratio barely consistent with the measured upper limit, and also for them the X-ray observed variability constrains the transition radius to be rather small (between ~ 20 and $100 R_S$).

The IR-to-X-ray Eddington ratio, the X-ray variability and spectral shape, and the radio-to-X-ray and NIR-to-X-ray luminosity ratios suggest that the nucleus of NGC4258 is an AGN in a low state (see e.g. Siemiginowska et al. 1996) or a scaled-down version of a Seyfert nucleus. This is also consistent with the conclusions of Neufeld & Maloney

(1995) who suggest that the low luminosity of NGC4258 is the result of low accretion rate ($\sim 10^{-4}M_{\odot}yr^{-1}$). In the model of Neufeld & Maloney (1995) the radiative efficiency is high, $\sim 10\%$, in contrast to the low efficiency ADAF models. The X-ray nuclear luminosity can be naturally explained in terms of Comptonization of soft photons in a hot corona (e.g. Haardt & Maraschi 1991, Haardt, Maraschi & Ghisellini 1994). Witt et al. (1997) developed a model of accretion disc plus corona introducing a coupling between the energy dissipated in the corona and the accretion rate. They found that if the viscosity mechanisms are the same in the disc and in the corona, the corona does not form for accretion rates smaller than a critical value, because Compton cooling wins against viscous heating in the corona. This critical value is $\dot{m}_c \approx 0.001$ at small radii and increases with the radius. Under this condition, if the Eddington ratio of 0.0002 is linearly proportional to \dot{m} and if the efficiency in the conversion of accretion power into radiation is $\eta \sim 0.1$, a corona should not form in the nucleus of NGC4258. There are at least two ways out from this problem. The first is that the efficiency η is at least as small as 0.01. This may be the case if a large part of the accretion power is carried out by a different channel, for example kinetic energy in a wind (as also foreseen in the Witt et al. model). Second, the dissipation of accretion power and the viscosity mechanisms may be very different in the disc and in the corona, as in the case of local magnetic reconnection flares in the corona, envisaged by Haardt, Maraschi & Ghisellini (1994).

More theoretical work is clearly needed to understand if accretion rates as small as 0.0002 in Eddington units may power a low luminosity version of a normal Seyfert galaxy nucleus, although this already seems for NGC4258 the most likely and less demanding, in terms of complexity, scenario.

5.2. Origin of the low energy component(s)

Makishima et al. (1994) and Ptak et al (1999) found some support for a two temperatures model for the low energy ASCA spectrum of this source. Using ROSAT HRI data Pietsch et al. (1994) and Cecil, Wilson & De Pree (1995) were able to resolve the soft X-ray emission in several components, the most relevant being a jet component. Cecil, Wilson and De Pree (1995) and Makishima et al. (1994) also report the discovery of a hotter thermal component ($kT \sim 4$ keV). The BeppoSAX data confirm the presence of at least two components, in addition to the obscured nuclear power law, in the 0.1-10 keV spectrum of this source. One component must be thermal, given the strong iron L complex detected, and its best fit temperature is $kT \sim 0.6$ keV. It can be due to shocks formed in the interaction of the jet with the interstellar matter (Cecil et al. 1995).

The shape of the second component is not well constrained by the BeppoSAX data. It is consistent with both thermal emission with temperature of $kT > 1.3$ keV or a power law with energy index $0.2^{+0.8}_{-0.2}$. This component may consist of a fraction of 0.935 ± 0.010 of the nuclear power law spilling out from a non uniform absorber. NGC4258 is known to be highly polarized (Wilkes et al 1995). This implies that there are lines of sight to the nucleus scattering photons towards us and providing an unobscured view. Such geometry mimicks a partial covering of the nuclear continuum. The observed covering fraction of is consistent with the 5–10 polarization observed in this source (Wilkes et al 1995). Alternatively, the second component may be due to integrated emission from binaries and Supernova Remnants. The contribution from these discrete sources may be estimated from the B band luminosity of NGC4258 (Trinchieri & Fabbiano 1985, Canizares, Trinchieri & Fabbiano 1987, Fabbiano et al. 1992). The total B magnitude, corrected for extinction, is $B=8.53$ (de Vaucouleurs et al 1991). This corresponds to a luminosity in the B band, in units of the solar luminosity, of $\log L_B=10.49$. The Fabbiano et al. (1992) relationship between L_X and L_B for normal spiral galaxies implies a 0.2-4 keV luminosity of 6×10^{39} erg s^{-1} from discrete sources, which is $\sim 70\%$ the measured “hot” component 0.2-4 keV luminosity. Since the scatter in the Fabbiano et al. (1992) correlation is a factor of three we cannot exclude that the entire observed “hot” component is due to discrete X-ray sources in the host galaxy. High spatial resolution observations, like those allowed by the superior telescopes on board the Chandra satellite, will be able to resolve the discrete sources in the galaxy and therefore measure or put strong limits to any truly diffuse “hot” component.

5.3. Strong X-ray absorption and water maser emission

The nuclear continuum of NGC4258 varies on a timescale of half a day (see Sect. 3). Our data are not good enough to detect Fe-K line variability. However, all the observations to date are consistent with Fe like flux being constant over at least few times 10^5 seconds. We also find that the flux of the Fe line is consistent with its origin in the absorbing gas (Sect. 4.1). All this places the Fe line, and so the absorber at a distance of $> 6 \times 10^{15}$ cm. The water maser emission in NGC4258 originates at 0.13 pc from the nucleus. Thus the location of the X-ray absorber is consistent with being the same as that of the maser emission. Such an association between the X-ray absorber and maser emission is further corroborated by a general tendency of maser sources to show strong X-ray absorption, see for example NGC4945 Circinus galaxy, NGC1068 (Matt. et al. 2000 and references therein), ESO103-G35 (Wilkes et al. 2001) and possibly NGC3079 (Bassani et al. 1999).

In the models of Neufeld & Maloney (1995) for maser emission in NGC4258, the

X-rays from the nuclear AGN are shielded by gas of large column density. Such shielding helps creating the layer of warm molecular gas in the midplane of the circumnuclear disk. The column density of the shielding gas in the Neufeld & Maloney (1995) model is $9 \times 10^{22} \text{ cm}^{-2}$, exactly what we measure in the present BeppoSAX observation. It is thus reasonable to assume that the large column density gas responsible for the nuclear X-ray absorption is also shielding the molecular gas. Neufeld & Maloney (1995) also note that if the circumnuclear disk is absolutely flat, i.e. not warped, then it would not be illuminated by the X-ray continuum. In this situation the temperature in the midplane of the disk would be too cold to excite water maser emission. Note that in such a geometry there would not be any X-ray absorption either.

All the above facts point towards a direct causal link between strong X-ray absorption and water maser emission. Illumination by X-ray continuum and subsequent shielding by a large column density gas seems to be required for maser emission, at least in some models. If such a scenario is correct, then every maser emitting AGN would show absorption in its X-ray spectrum.

We would like to thank the BeppoSAX hardware teams for the development and calibration of the instruments. In particular, we would like to remember the late Daniele Dal Fiume for his continuous dedication and his fundamental contribution to an instrument of unprecedented sensitivity and robustness like the BeppoSAX PDS.

This research has made use of SAXDAS linearized and cleaned event files (Rev.2.0) produced at the BeppoSAX Science Data Center. It has been partially supported by ASI contract ARS-99-75 and MURST grant Cofin-98-032. SM work has been partly supported by the NASA grant NAG5-8913 (LTSA). We thank Tiziana Di Matteo, Fabrizio Nicastro and Massimo Cappi for useful discussions.

REFERENCES

- Bassani, L. et al. 1999, *ApJS*, 121, 473
Blandford, R.D., Begelman, M.C., 1999, *MNRAS*, 303, L1
Canizares, C.R., Fabbiano, G. & Trinchieri, G. 1987, *ApJ*, 312, 503
Cecil, G., Wilson, A.S., & De Pree, C. 1995, *ApJ*, 440, 181
Chary, R. & Becklin, E.E. 1997, *ApJL*, 485, L75
de Vaucouleurs, G., de Vaucouleurs, A., Corwin, H.G., Buta, R.J., Paturel, G., Fouqué, P. 1991, *Third Reference Catalogue of Bright Galaxies* (Springer, New York)

- Di Matteo, T., Quataert, E., Allen, S.W. Narayan, R. & Fabian, A.C., 2000, MNRAS, 311, 507
- Elvis, M., Wilkes, B.J., McDowell, J.C., Green, R.F., Bechtold, J., Willner, S.P., Polomski, E. & Cutri, R. 1994, ApJS, 95, 1
- Fabbiano, G., Kim, D.-W., Trinchieri, G, 1992, ApJS, 80, 531
- Fiore, F., Guainazzi, M. & Grandi, P. 1999, Handbook for BeppoSAX NFI spectral analysis, ftp://www.sdc.asi.it/pub/sax/doc/software_docs/saxabc_v1.2.ps.gz
- Falke, H. & Biermann, P.L. 1999, A&A, 342, 49
- Gammie, C.F., Narayan, R. & Blandford, R., 1999, ApJ, 516, 177
- Green, A.R., McHardy, I.M., Letho, H.J. 1993, MNRAS, 265, 664
- Haardt, F. & Maraschi, L. 1991, ApJL, 380, L51
- Haardt, F., Maraschi, L. & Ghisellini, G. 1994, ApJL, 432, L95
- Herrnstein, J.R., et al. 1998, ApJ, 497, 69
- Herrnstein, J.R., Moran, J.M., Greenhill, P.J.T., Diamond, P.J., Inoue, M., Nakai, N., Miyoshi, M., Henkel, C., Riess, A., 1999, Nature, 400, 539
- Ho, L.C., Filippenko, A.V., & Sargent, W.L.W. 1997, ApJS, 112, 391
- Lasota, J.-P., Abramowicz, M.A., Chen, X., Krolik, J., Narayan, R. & Yi, I. 1996, ApJ, 462, 142
- Makishima, K. et al. 1994, PASJ, 46, L77
- Matt., G. 2000, Astr. Lett. and Comm. in press, proceedings of the Bologna meeting “X-ray Astronomy ’999, Stellar Endpoints, AGN and the Diffuse Background”, astro-ph/0007105
- Matt G., Fabian A.C., Guainazzi M., Iwasawa K., Bassani L., Malaguti G., 2000, MNRAS, 318, 173
- Miyoshi, M., Moran, J., Herrnstein, J., Greenhill, L., Nakai, N., Diamond, P., & Inoue, M. 1995, Nature, 373, 127
- Nandra, K., George, I.M., Mushotzky, R.F., Turner, T.J., Yaqoob, T., 1997, ApJ, 476, 70
- Narayan, R. & Yi I., 1995, ApJ, 444, 231
- Narayan, R, Mahadevan, R. & Quataert E. 1998, in in ”The Theory of Black Hole Accretion Discs”, eds. M. A. Abramowicz, G. Bjornsson, and J. E. Pringle, astro-ph/9803141
- Neufeld, D.A. & Maloney, P.R., 1995, ApJL, 447, 17
- Ptak, A., Serlemitsos, P. Yaqoob, T. & Mushotzky, R. 1999, ApJS, 120, 179

- Quataert, E. & Narayan, R. 1999, ApJ, 520, 298
- Reynolds, C.S., Nowak, M.A., & Maloney, P.R. 2000, ApJ, 540, 143
- Siemiginowska, A., Czerny, B. & Kostyunin, V. 1996, ApJ, 458, 491
- Trinchieri, G. & Fabbiano, G. 1985, ApJ, 296, 447
- Wilkes, B.J., Schmidt, G. D., Smith, P.S., Mathur, S. & McLeod, K.K. 1995, ApJ, 455, L13
- Wilkes, B.J., Mathur, S., Fiore, F., Antonelli, L.A., Nicastro, F. 2001, ApJ in press, astro-ph/0010429
- Witt, H.J., Czerny, B., & Życki, P.T. 1997, MNRAS, 286, 848
- Zdziarski, Andrzej A., Poutanen, Juri, Johnson, W. Neil, 2000, ApJ, 542, 703

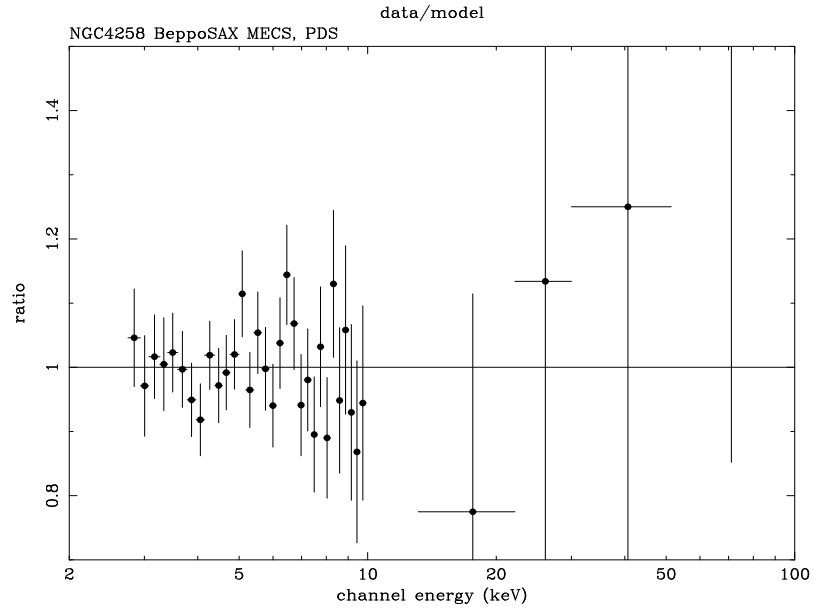


Fig. 4.— The ratio between the MECS and PDS 2.5-100 keV data and the best fitting absorbed power law model given in Table 2.

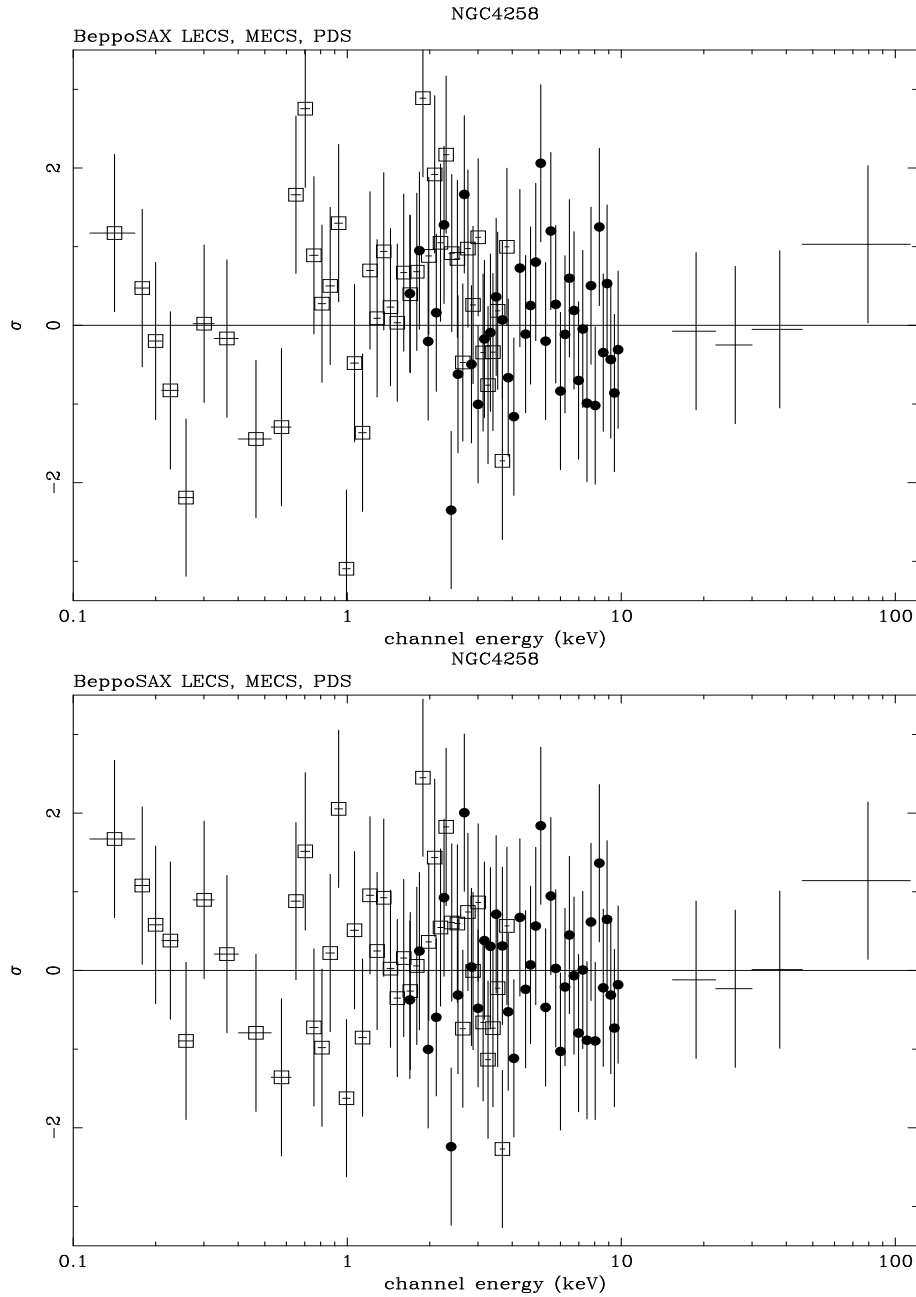


Fig. 5.— Upper panel, the residuals, in number of σ , after the subtraction of the best fit single MEKAL plus power law model from the LECS (open squares), MECS (filled circles) and PDS (crosses) data. Note the relatively large deviations around 0.7 and 1 keV; lower panel, same as in the upper panel but for a model including two thermal components. The residuals do not show any large deviation in the whole 0.1-100 keV band.

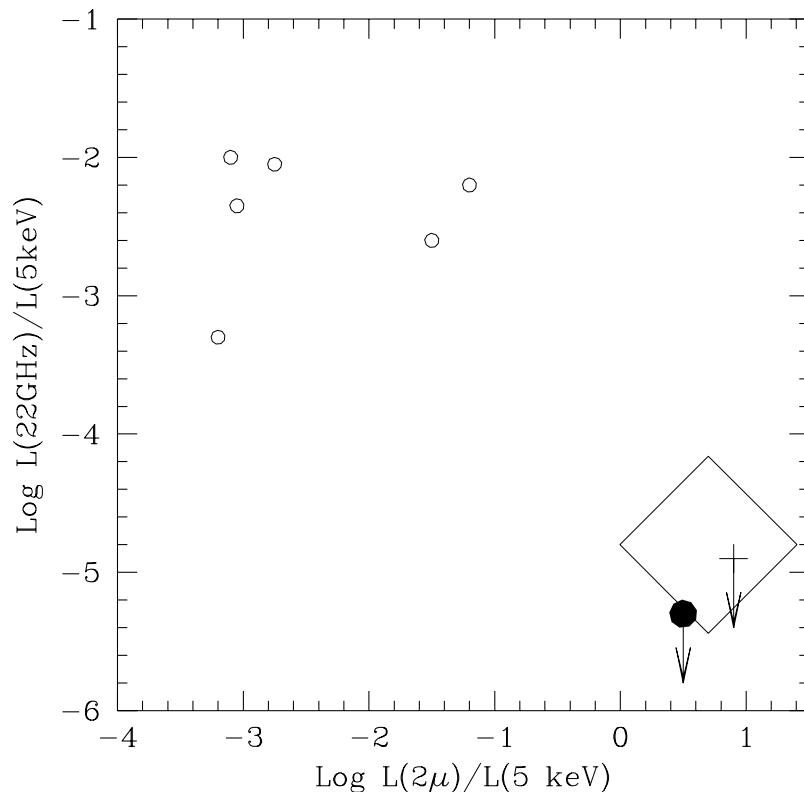


Fig. 6.— The ratio between the 22GHz luminosity to the 5 keV luminosity as a function of the ratio between the 2 micron luminosity and the 5 keV luminosity. Big diamond = area covered by the radio quiet quasar SEDs of Elvis et al. (1994); filled circle = NGC4258, BeppoSAX observation; cross = NGC4258, ASCA observations (average); open circles = best fit ADAF plus wind models to the six elliptical galaxies studied by Di Matteo et al. (2000). It should be noted that while the X-ray and the radio luminosities of the six models are very close to measured values, the NIR points come just from the models.